International Journal For Advanced Research In Science & Technology
A peer reviewed international journal
www.ijarst.in
ISSN: 2457-0362

CONVENTIONAL MAXIMUM POWER POINT TRACKING TECHNIQUES FOR SOLAR PHOTO VOLTAIC GRID-CONNECTED INVERTER BASED ON VOLTAGE-ORIENTED CONTROL

CHAVAPATI GOUSEPEERA VALI[1], K.ASHOK KUMAR[2]
[1]PG SCHOLAR, DEPT OF EEE, ESWAR COLLEGE OF ENGINEERING, NARASARAOPET, AP, INDIA
[2]PROJECT SUPERVISOR, ASSOCIATE PROFESSOR, DEPT OF EEE, ESWAR COLLEGE OF ENGINEERING, NARASARAOPET, AP, INDIA
chavapatigouse@gmail.com, kolluruashok206@gmail.com

ABSTRACT: Adaptable force point following (FPPT) is the control of dynamic force created by network associated photovoltaic force plants (GCPVPPs) to give framework uphold usefulness. A FPPT calculation for the decrease of the separated force from photovoltaic (PV) strings during voltage droops was recently proposed by the creators. A favorable position of this calculation, contrasted with customary FPPT calculations, was its quick elements encouraged by utilization of a basic PI regulator that progressively changes the PV voltage reference. The recently proposed plan must be utilized for the brief length in which the force framework encounters voltage list. A tale change to this calculation with multi-mode activity is presented in this letter, which gives FPPT ability to nonstop activity of GCPVPPs. In contrast to the past calculation, which had the option to just move the activity highlight the right-hand side of MPP, the proposed calculation in this letter can move the activity highlight both right and left-hand sides of the MPP that gives the adaptability to work in the ideal activity district for both single- and two-stage GCPVPPs. Exploratory outcomes are given to exhibit the presentation of the proposed calculation under unique irradiance conditions.

1.INTRODUCTION

Adaptable force point following (FPPT) calculations have been created to give recurrence backing and low-voltage ride-through (LVRT) capacities for lattice associated photovoltaic force plants (GCPVPPs) [1]. The standards of FPPT are exhibited in Fig. 1. Dissimilar to most extreme force point following (MPPT) calculations, which consistently separate the accessible greatest force (pmpp) from the PV strings, by working at the most extreme force point (MPP) in Fig. 1(a), the FPPT calculations manage the PV power (ppv) to a force reference (pfpp), got from an upper level control framework, by working the PV strings at focuses An or B in Fig. 1(a). Besides, by applying FPPT calculations, the infused dynamic capacity to the lattice can be decreased during framework voltage lists, to give responsive force infusion ability dependent on the network necessities. Also, power incline rate control can be accomplished by applying FPPT calculations in GCPVPPs [2]. Different FPPT calculations are presented in the writing with different preferences and detriments [3], [4]. It is noticed that GCPVPPs with FPPT usefulness are needed to be larger than average, contrasted with the GCPVPPs with MPPT usefulness, however

International Journal For Advanced Research In Science & Technology
A peer reviewed international journal
www.ijarst.in
ISSN: 2457-0362

with the additional advantages of framework uphold usefulness.

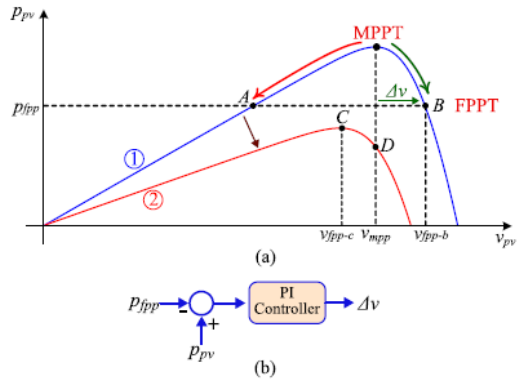

Fig. 1. Principles of flexible power point tracking in GCPVPPs. (a) Powervoltage curve under various operation conditions. (b) Algorithm for the calculation of Δv.

A few FPPT calculations for the activity of two-stage GCPVPPs (those with incorporated dc–dc converters) during voltage droops have been proposed in [5]–[7]. The infusion of receptive capacity to the lattice, in light of the matrix code necessities, may force a decrease in the infused dynamic ability to abstain from surpassing the greatest current rating of the inverter. In these proposed calculations, the MPPT calculation stops its activity during framework voltage hangs, though the control stage records the last determined voltage reference related with the MPP, preceding the discovery of the voltage list. To control the PV capacity to the necessary force reference during the voltage list, the activity purpose of the PV strings is moved to one side hand side of the MPP, by adding an extra voltage Δv to the last recorded MPP voltage, as demonstrated in Fig. 1(a). The estimation of Δv is determined by a relative essential (PI) regulator, as demonstrated in Fig. 1(b). The contribution of the PI regulator is the blunder between the PV power ppv and power reference pfpp [6], or the mistake between the dc-connect voltage and its reference [5], [7]. The primary bit of leeway of the calculations in [5]–[7], contrasted with other accessible FPPT calculations in the writing [3], [4], is quick unique execution. This is accomplished with the utilization of a PI regulator that adaptively ascertains the PV voltage reference. In traditional FPPT calculations, for example, those dependent on the irritate and notice (P&O) calculation, a steady voltage-venture with low-recurrence estimation transfer speed (for example 1–20Hz in useful applications) is typically applied. For this situation, quick elements can be achieved by utilizing a moderately huge voltage-step. Be that as it may, enormous voltage-step esteems bring about huge force motions at consistent state. In the calculations in [5]–[7], it is accepted that the span of the matrix voltage droop is moderately short (_150 ms) and that there is no huge change in natural conditions (irradiance, temperature, and so on) during this period, which implies that the MPP voltage stays consistent. The accompanying model shows why these calculations can't guarantee the extraction of steady force from PV strings throughout significant time-frame periods, in which winning natural conditions change. In Fig. 1, at first, the force voltage (P-V) bend of the PV board is curve_1 . The PV works at point B, accomplished by adding Δv to the last recorded MPP voltage (vmpp) before the event of the voltage droop. Because of unexpected ecological changes, the P-V bend changes to bend _2 . In this condition, the fitting FPPT activity point is C, in light of the fact that the most extreme accessible PV power is more modest than pfpp. Nonetheless, the calculations in [5]–[7] can't follow the

International Journal For Advanced Research In Science & Technology
A peer reviewed international journal
www.ijarst.in
ISSN: 2457-0362

voltage of point C. This is on the grounds that the MPP voltage is thought to be steady at vmpp and the mistake among ppv and pfpp is positive, which brings about a huge positive Δv in the yield of the PI regulator, as demonstrated in Fig. 2

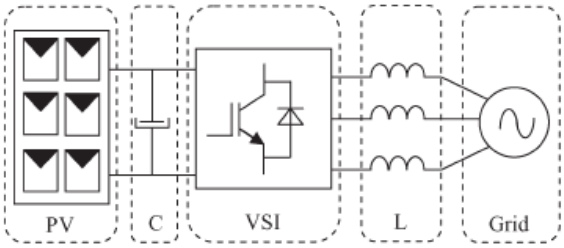

Fig 2. . Typical configuration of a single-stage grid-connected PV system.

As needs be, the calculation will keep the activity point past the open-circuit voltage of the PV string. Hence, these calculations can't guarantee the constant FPPT activity of GCPVPPs. To expand the pertinence of these calculations for consistent activity, a multi-mode-based FPPT is proposed in this letter. In one activity mode, a traditional MPPT calculation is performed to expand the PV power, while in the second activity mode, a PI regulator is executed to lessen the PV power toward its ideal worth. The proposed calculation is additionally material for both single-and two-stage GCPVPPs, on the grounds that it can move the activity highlight the right-or left-hand sides of the MPP.

2 LITERATURE SURVEY

H. D. Tafti, A. Sangwongwanich, Y. Yang, J. Pou, G. Konstantinou, and F. Blaabjerg,One of the significant concerns related with the expanding infiltration of network associated photovoltaic (PV) power plants is the operational difficulties (e.g., over-burdening and overvoltage), forced because of the fluctuation of PV power age. An adaptable force point following (FPPT), which can restrict the PV yield capacity to a particular worth, has accordingly been characterized in lattice association guidelines to handle a portion of the joining testing issues. Nonetheless, the traditional FPPT calculation dependent on the bother and notice technique experiences moderate elements. In this paper, a versatile FPPT calculation is subsequently proposed, which highlights quick elements under quickly changing ecological conditions (e.g., because of passing mists), while keeping up low force motions in consistent state. The proposed calculation utilizes an extra estimated examining at every irritation to notice the adjustment in the working condition (e.g., sunlight based irradiance). A short time later, the voltage-step is adaptively determined after the noticed condition (e.g., transient or consistent state) in an approach to improve the following exhibition. Exploratory outcomes on a 3-kVA lattice associated single-stage PV framework approve the viability of the proposed calculation as far as quick elements and high exactness under different operational conditions.

H. D. Tafti,Low-voltage ride-intensive ability is among the difficulties in the activity of medium-and huge scope lattice associated photovoltaic force plants (PVPPs). Moreover, responsive force infusion during voltage hangs is needed by power framework administrators to improve the voltage of the purpose of normal coupling. The presentation of medium-and enormous scope framework associated PVPPs during these occasions is contemplated. A calculation for the count of current references, in the dq-outline, during voltage droops is presented, which thinks about the inverter current restriction, lattice

International Journal For Advanced Research In Science & Technology
A peer reviewed international journal
www.ijarst.in
ISSN: 2457-0362

code prerequisites and the measure of separated force from photovoltaic strings. The proposed calculation utilizes the full current limit of the inverter in infusing dynamic or responsive forces to the network during voltage droops, which leads in a superior lattice voltage improvement. The exhibition of proposed control methodologies is examined on a 150-kVA PVPP associated with the 12.47-kV medium-voltage experiment framework reenactment model during various shortcoming conditions. An exploratory arrangement of the 3.3-kVA lattice associated three-level nonpartisan point-braced inverter with a dc/dc converter shows and approves the presentation of the regulator in infusing required dynamic/receptive force and supporting the organization voltage.

3.SYSTEM DESCRIPTION AND MODELING

This framework comprises of a PV cluster, an info channel capacitor C, a three-stage VSI, a yield channel inductor L, and network. The PV modules are associated in an arrangement equal design to coordinate the necessary dc voltage and force rating. The information capacitor underpins the sun oriented cluster voltage for the VSI. The three-stage beat width-tweaked inverter with a channel inductor changes over a dc input voltage into an air conditioner sinusoidal voltage by methods for fitting change signs to make the yield current in stage with the utility voltage and get a solidarity power factor.

A. Solar Cell and PV Array Model

A PV generator is a blend of sun oriented cells, associations, defensive parts, upholds, and so on In the current displaying, the emphasis is just on cells. Sunlight based cells comprise of a p-n intersection; different modelings of sun based cells have been proposed in the writing.

Accordingly, the least complex identical circuit of a sun oriented cell is a current source in corresponding with a diode. The yield of the current source is straightforwardly corresponding to the light falling on the cell (photocurrent). During dimness, the sun powered cell is certainly not a functioning gadget; it fills in as a diode, i.e., a p-n intersection. It produces neither a current nor a voltage. Consequently, the diode decides the I–V qualities of the cell. For this paper, the electrical identical circuit of a sun based cell is appeared in Fig. 2 The yield current I and the yield voltage of a sun powered cell are given by

$$I = I_{\text{ph}} - I_{do} - \frac{V_{do}}{R_{\text{sh}}}$$

$$= I_{\text{ph}} - I_0\left(\exp\left(\frac{q.V_{do}}{n.k.T}\right) - 1\right) - \frac{V_{do}}{R_{\text{sh}}} \quad (1)$$

$$V = V_{do} - R_s I. \quad (2)$$

Here, Iph is the photocurrent, I0 is the reverse saturation current, Id0 is the average current through the diode, n is the diode factor, q is the electron charge (q = 1.6∗10−19), k is

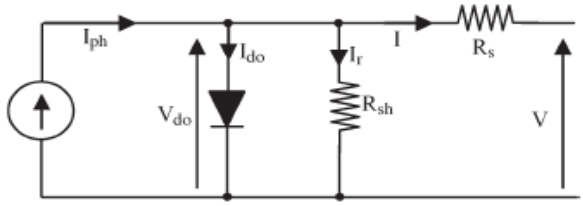

Fig. 3. Solar cell electrically equivalent circuit.

International Journal For Advanced Research In Science & Technology
A peer reviewed international journal
www.ijarst.in
ISSN: 2457-0362

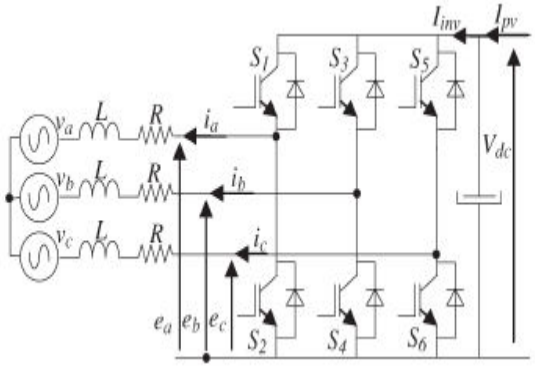

Fig. 4. Three-phase VSI.

The Boltzmann's constant (k = 1.38∗10−23), and T is the solar array panel temperature. Rs is the intrinsic series resistance of the solar cell; this value is normally very small. Rsh is the equivalent shunt resistance of the solar array, and its value is very large. In general, the output current of a solar cell is expressed by

$$I = I_{\text{ph}} - I_0\left(\exp\left(\frac{q}{n.k.T}(V + R_s I)\right) - 1\right) - \left(\frac{V + R_s I}{R_{\text{sh}}}\right). \tag{3}$$

In (3), the resistances can be generally neglected, and thus, it can be simplified to

$$I = I_{\text{ph}} - I_0\left(\exp\left(\frac{q}{n.k.T}.V\right) - 1\right). \tag{4}$$

If the circuit is opened, the output current I = 0, and the open-circuit voltage Voc is expressed by

$$V_{\text{oc}} = \left(\frac{n.k.T}{q}\right) In\left(\frac{I_{\text{ph}}}{I_0} + 1\right) \approx \left(\frac{n.k.T}{q}\right) In\left(\frac{I_{\text{ph}}}{I_0}\right). \tag{5}$$

If the circuit is shorted, the output voltage V = 0, the average current through the diode is generally neglected, and the short circuit current Isc is expressed by using

$$I_{\text{sc}} = I = \frac{I_{\text{ph}}}{\left(1 + \frac{R_s}{R_{\text{sh}}}\right)}. \tag{6}$$

Finally, the output power P is expressed by

$$P = VI = \left(I_{\text{ph}} - I_{do} - \frac{V_{do}}{R_{\text{sh}}}\right)V. \tag{7}$$

A. VSI Model

The VSI associated with the lattice through a L channel is appeared in Fig. 3. In this segment, a powerful insightful model of the VSI is created in its unique three-stage abc outline. At that point, this model is changed into a simultaneous reference outline. Prior to breaking down the three-stage VSI, a few suppositions are proposed.

1) The three-stage voltages are sinusoidal and balanced, and their portrayals are portrayed in (8).

2) The switches work at consistent recurrence. The exchanging recurrence is a lot higher than the line recurrence.

3) The inductors L are straight and adjusted. Immersion isn't a worry.

4) The entire conduction misfortunes are addressed by three balanced resistors R, as demonstrated in Fig. 3.

5) The shortfall of the zero grouping in the flows into a three wire framework.

$$\begin{cases} \nu_a = V_m \cos(\omega t) \\ \nu_b = V_m \cos\left(\omega t - \frac{2}{3}\pi\right) \\ \nu_c = V_m \cos\left(\omega t + \frac{2}{3}\pi\right). \end{cases} \tag{8}$$

Based on the aforementioned assumptions, the model of the VSI in the stationary abc frame is established as

$$\begin{cases} e_a = L\frac{di_a}{dt} + i_a R + \nu_a + \nu_{nN} \\ e_b = L\frac{di_b}{dt} + i_b R + \nu_b + \nu_{nN} \\ e_c = L\frac{di_c}{dt} + i_c R + \nu_c + \nu_{nN} \\ I_{pv} = C\frac{dV_{\text{dc}}}{dt} + I_{\text{inv}}. \end{cases} \tag{9}$$

By doing the sum of the three equations in (9), one can obtain the relation

$$\nu_{nN} = \frac{1}{3}(e_a + e_b + e_c). \tag{10}$$

International Journal For Advanced Research In Science & Technology
A peer reviewed international journal
www.ijarst.in
ISSN: 2457-0362

The switching function d∗k (k = 1, 3, 5) of the inverter is defined as in

$$d_k^* = \begin{cases} 1, & \text{if } S_k \text{ is on and } S_{k+1} \text{ is off} \\ 0, & \text{if } S_k \text{ is off and } S_{k+1} \text{ is on.} \end{cases} \quad (11)$$

Hence, one can write the complete model (12) of the VSI in the abc frame

$$\begin{cases} L\frac{di_a}{dt} = -\nu_a - i_a R + \left(d_1^* - \frac{d_1^*+d_2^*+d_3^*}{3}\right) V_{\rm dc} \\ L\frac{di_b}{dt} = -\nu_b - i_b R + \left(d_2^* - \frac{d_1^*+d_2^*+d_3^*}{3}\right) V_{\rm dc} \\ L\frac{di_c}{dt} = -\nu_c - i_c R + \left(d_3^* - \frac{d_1^*+d_2^*+d_3^*}{3}\right) V_{\rm dc} \\ C\frac{dV_{\rm dc}}{dt} = I_{pv} - (d_1^* i_a + d_2^* i_b + d_3^* i_c)\,. \end{cases} \quad (12)$$

For pulsewidth modulation (PWM) inputs, the aforementioned model can be separated into low- and high-frequency components using the Fourier analysis. The high-frequency model is concerned with the switching behavior of the inverter and is almost neglected. The low-frequency model, which has the same expression as (12), with the switching functions d∗ being replaced by continuous duty ratios dk(k = 1, 3, 5) ∈ [0, 1], is much more considered

$$T_{dqo}^{abc} = \frac{2}{3}\begin{bmatrix} \cos(\omega t) & \cos\left(\omega t - \frac{2}{3}\pi\right) & \cos\left(\omega t + \frac{2}{3}\pi\right) \\ \sin(\omega t) & \sin\left(\omega t - \frac{2}{3}\pi\right) & \sin\left(\omega t + \frac{2}{3}\pi\right) \\ \frac{1}{2} & \frac{1}{2} & \frac{1}{2} \end{bmatrix}. \quad (13)$$

It is noted that the model (12) is time varying and nonlinear. In order to facilitate the control, the model can be transformed into a synchronous orthogonal frame rotating at the angular frequency of the utility ω. With this time-varying transformation, given by (13), the positive sequence components at the fundamental frequency become constant.

Finally, the whole dynamic model (14) in the dq frame is obtained from (12) and (13)

$$\begin{bmatrix} \frac{di_d}{dt} \\ \frac{di_q}{dt} \\ \frac{dV_{\rm dc}}{dt} \end{bmatrix} = \begin{bmatrix} -\frac{R}{L} & \omega & \frac{d_d}{L} \\ -\omega & -\frac{R}{L} & \frac{d_q}{L} \\ -\frac{d_d}{C} & -\frac{d_q}{C} & 0 \end{bmatrix} \begin{bmatrix} i_d \\ i_q \\ \nu_{\rm dc} \end{bmatrix} + \begin{bmatrix} -\frac{1}{L} & 0 & 0 \\ 0 & -\frac{1}{L} & 0 \\ 0 & & \frac{1}{C} \end{bmatrix} \begin{bmatrix} \nu_d \\ \nu_q \\ I_{pv} \end{bmatrix} \quad (14)$$

Where id, iq d- and q-axis grid currents, respectively; vd, vq d- and q-axis grid voltages, respectively; dd, dq d- and q-axis duty ratios.

4.CURRENT AND VOLTAGE CONTROLLERS

According to [19], VOC strategy guarantees fast transient response and high static performance via internal current control loops.

A. Current Control

It can be seen from (14) that there is cross-coupling between the d and q components. However, cross-coupling can affect the dynamic performance of the regulator. Therefore, it is very important to decouple the two axes for better performance. This effect can be accomplished with the feed forward decoupling control method. Assuming that

$$\begin{aligned} \nu_{rd} &= -V_d + d_d V_{\rm dc} + \omega L i_q \\ \nu_{rq} &= -V_q + d_q V_{\rm dc} - \omega L i_d \end{aligned} \quad (15)$$

where ω is the angular frequency of the utility. Then, the system model is transformed to

$$\begin{cases} \frac{di_d}{dt} = -\frac{R}{L} i_d + \frac{1}{L}\nu_{rd} \\ \frac{di_q}{dt} = -\frac{R}{L} i_q + \frac{1}{L}\nu_{rq} \\ \frac{dV_{\rm dc}}{dt} = \frac{I_{pv}}{C} - \frac{V_d+\nu_{rd}}{CV_{\rm dc}} i_d - \frac{V_q+\nu_{rq}}{CV_{\rm dc}} i_q. \end{cases} \quad (16)$$

The cross-coupling variables are eliminated in the aforementioned model. Hence, the currents id and iq can be controlled independently by acting upon inputs Vd and Vq, respectively.

International Journal For Advanced Research In Science & Technology
A peer reviewed international journal
www.ijarst.in
ISSN: 2457-0362

Furthermore, by using PI-type regulators, a fast dynamic response and zero steady-state errors can be achieved. The diagram of the current regulator is shown in Fig. 4. Since the switching frequency is much higher than the line frequency, the sampling and hold delay is neglected.

the diagram, kip and kii are the proportional and integral parameters, respectively; i∗ is the reference current signal, and I is the feedback current. The diagram is suitable for both id and

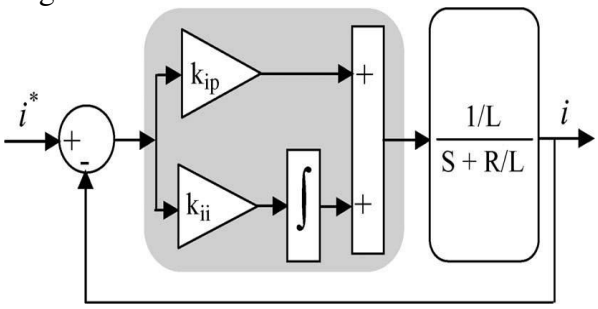

Fig. 5. Diagram of the current loop.

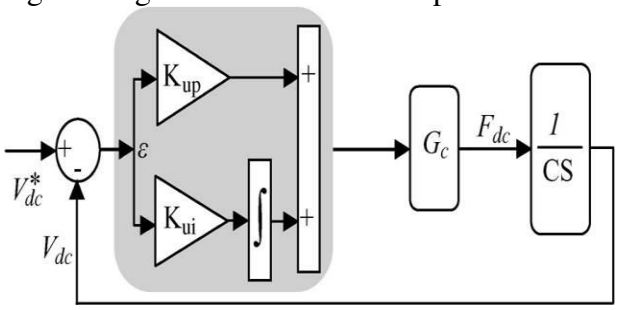

Fig. 6. Voltage loop diagram with constant irradiation.

iq loops. From the diagram, the closed-loop transfer function of the d, q current loops is

$$\frac{i_q(s)}{i_q^*(s)} = \frac{i_d(s)}{i_d^*(s)} = \frac{k_{ip}}{L} \frac{S + \frac{k_{ii}}{k_{ip}}}{S^2 + \frac{(k_{ip}+R)}{L} S + \frac{k_{ii}}{L}}. \quad (17)$$

The damping ratio ζ = (kip + R)/2L_kii/L, and ω2 ni = kii/L. Thus, the parameters of the current regulator can be designed as follows:

kip =2ζωniL − R
kii =Lω2 ni. (18)

B. Voltage Control

In the case of a unity power factor (iq = 0) and with the previous assumption, the third equation in the model (14) is repeated as

$$C\frac{dV_{dc}}{dt} = I_{pv} - d_d i_d. \quad (19)$$

At the beginning of a sequence, the atmospheric conditions are considered constant; hence, an equivalent input is defined as

$$F_{dc} = I_{pv} - d_d i_d. \quad (20)$$

In order to regulate the dc voltage at a fixed value, the error ε = V ∗ dc − Vdc is passed through a PI-type compensator, as shown in Fig. 5.

In the diagram, the voltage loop is an outer loop, while the current loop is an inner loop. The internal loop has been designed to achieve short settling times in order to achieve a fast correction of the error. The outer loop can be designed to be slower. Thus, the inner and outer loops can be considered decoupled, and they can be linearized. Consequently, the current loop transfer function is approximately considered as Gc = 1.

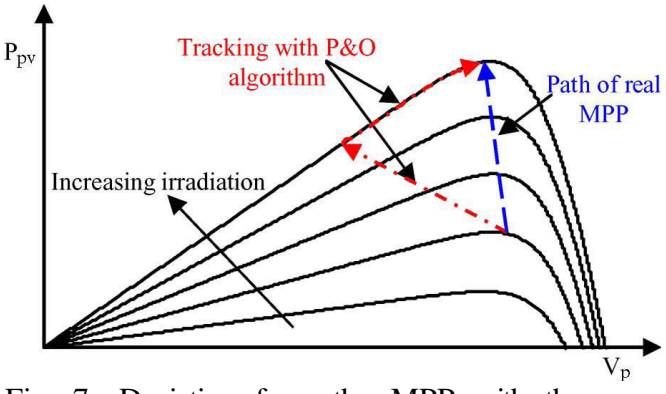

Fig. 7. Deviation from the MPP with the P&O algorithm under rapidly changing irradiance.

International Journal For Advanced Research In Science & Technology
A peer reviewed international journal
www.ijarst.in
ISSN: 2457-0362

The closed-loop transfer function of dc voltage regulation, obtained from Fig. 5, has the following form:

$$\frac{V_{dc}(s)}{V_{dc}^{*}(s)} = \frac{k_{up}}{C} \frac{\frac{k_{ui}}{k_{up}} + S}{S^2 + \frac{k_{up}}{C} S + \frac{k_{ui}}{C}}. \quad (21)$$

In the same way as the design process of the current loop, the voltage regulator parameters can be given as follows:

$$k_{up} = 2\zeta C \omega_{nu}$$
$$K_{ui} = C\omega_{nu}^2. \quad (22)$$

5.PROPOSED FPPT

The control diagram of the proposed multi-mode FPPT algorithm is shown in Fig. 2. There are two operation modes, depending on the relation between the PV power ppv and power reference pfpp, as follows.

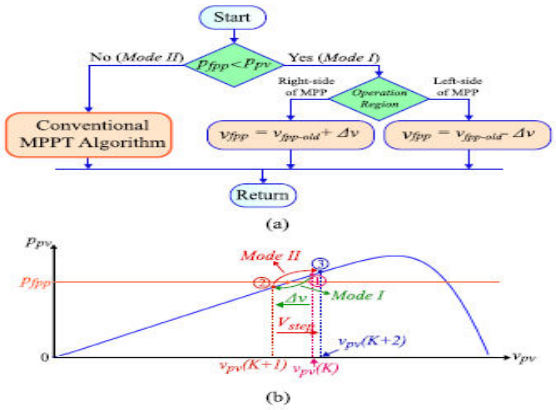

Fig. 8. Proposed multi-mode FPPT algorithm. (a) Control diagram of the algorithm. (b) Demonstration of the multi-mode operation.

Mode I (pfpp ≤ ppv): In this mode, the PVpower ought to be diminished. To diminish the force, the MPPT calculation stops its activity and the last recorded MPP voltage reference (vfppold) is utilized, as outlined in Fig. 2(a). For the activity in the left-hand side ofMPP, the decrease of the PV power is accomplished by subbing the determined Δv from vfppold (Vf pp =Vvfppold − Δv). As demonstrated in Fig. 1(b), Δv is determined utilizing a PI regulator. The contribution of this PI regulator is the blunder between the PV power Ppv and force reference Pfpp, which is determined on a high recurrence figuring data transmission (e.g., estimation transfer speed of the control stage). Moreover, for a moderately huge mistake esteem, Δv turns out to be generally enormous, which moves the activity highlight its ideal point in a brief timeframe span. This component brings about quick powerful execution of the proposed calculation. On the off chance that the PV activity point is near its reference point, the blunder is little, which adds to a generally little incentive for Δv. Thusly, just little force motions around the working point are acquired during consistent state. It ought to be referenced that PV voltage is changed with a high-recurrence computation transfer speed (the count recurrence data transmission of the regulator stage, e.g., 100 kHz) in the proposed calculation, which brings about quick elements contrasted with ordinary FPPT calculations with moderately low estimation data transfer capacity. This mode is exhibited in Fig. 2(b). At t = KT, where K is the quantity of the count step and T is the figuring time step, the PV voltage is vpv(K) at point_1 . Now, ppv is bigger than pfpp, consequently the proposed calculation diminishes the PV voltage by taking away its past an incentive by Δv, as examined already. Because of the decrease of the PV voltage, the activity guide advances toward point _2 , which delivers less force, contrasted with pfpp.

Mode II (pfpp > ppv): In this mode, the calculation expands the PV power by initiating the MPPT calculation, as demonstrated in Fig. 2. Any traditional

International Journal For Advanced Research In Science & Technology
A peer reviewed international journal
www.ijarst.in
ISSN: 2457-0362

MPPT calculation can be sent. In this examination, P&O MPPT calculation is actualized. It depends on a stage change of the PV voltage (Vstep) in every count step and assurance of the heading of the following voltage change, in view of the PV power change. The boundary Δv isn't added to the voltage reference determined by the MPPT calculation in this condition. Consequently, the MPPT calculation builds the PV power toward pfpp. This activity is appeared in Fig. 2(b). At t = (k + 1)T, vpv = vpv(K + 1) and the activity point is at_2 with ppv < pfpp. As needs be, the proposed calculation works in Mode II and the MPPT calculation builds the PV power by adding a voltage-step Vstep to the PV reference voltage. Because of this activity, the activity direct pushes toward _3 , with higher force than pfpp, as demonstrated in Fig. 2(b). It is noticed that actualizing a MPPT calculation in Mode II doesn't imply that the activity point is moved to the most extreme force point. It just implies that the PV power is expanded by moving the activity highlight the most extreme force (point _3). The multi-mode activity highlight of the proposed calculation encourages ceaseless activity ability. Not at all like the calculations in [5]–[7], the MPPT activity isn't stopped during the FPPT activity and all things considered, it is executed as one of the activity modes. In the event that the PV power decreases than pfpp, because of ecological changes or varieties in pfpp from an upper level regulator, Mode II is enacted, which expands the PV power by means of the MPPT activity.

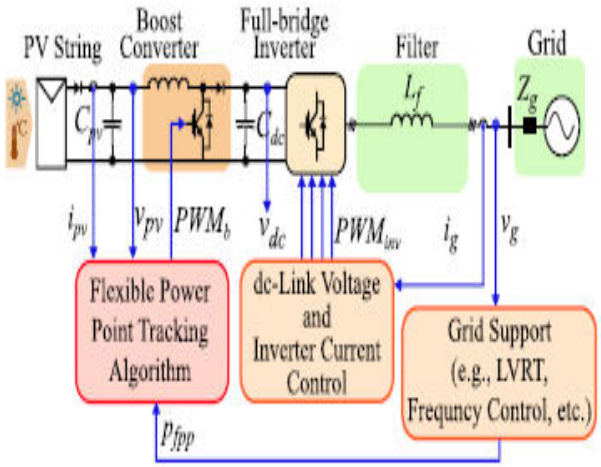

Fig. 9. Circuit diagram of experimental verification on a down-scaled twostage GCPVPP.

The proposed calculation is additionally ready to move the activity highlight the right-hand side of the MPP. The solitary contrast is that during Mode I activity, the worth Δv ought to be added to vfppold, rather than being deducted from it. It ought to be referenced that the determination of the advanced activity areas ought to be performed by a more significant level regulator and isn't the principle focal point of this investigation. The FPPT activity in the right-hand side of MPP gives quicker unique execution contrasted with the left-hand side of MPP, in light of the fact that a little change in the voltage brings about a huge difference in force. Then again, the activity in the right-hand side of MPP brings about bigger force motions contrasted with the left-hand side of MPP. This ought to be considered in the plan of the PI control boundaries.

6.SIMULATION RESULTS

The exhibition of the proposed multi-mode FPPT calculation is assessed on a downsized

International Journal For Advanced Research In Science & Technology
A peer reviewed international journal
www.ijarst.in
ISSN: 2457-0362

two-stage GCPVPP. The circuit chart of the framework is appeared in Fig. 3. It comprises of a dc–dc help converter with FPPT usefulness and a network associated inverter, which directs the dc-connect voltage to its ideal worth and conforms to matrix code prerequisites. The force reference pfpp is determined with the regulator of the network associated inverter. The PV board is reenacted utilizing the Chroma 62000H-S sun based exhibit test system. The most extreme force of the PV board at irradiance of Irr = 1000 W/m2 and temperature of T = 25 °C is pmpp = 800W (vmpp = 110V and impp = 7.3A). The lattice voltage (vrms = 70 V) is blend utilizing a Cinergia network emulator. The dc–ac inverter and dc–dc converters are actualized utilizing Imperix full-connect modules. The dc-interface voltage is 170V and the regulator is actualized on the Boom box control stage. Two contextual investigations with the development of activity highlight the right-and left-hand sides of the MPP are performed under quick irradiance changes. To confirm the exhibition of the calculation proposed in this letter (alluded to as Method 1), the outcomes are contrasted and the calculation of [3], [8], and [9] (alluded to as Method 2). In Method 2, the PV voltage reference is determined straightforwardly by means of a FPPT calculation, which depends on the adjustment of the P&O calculation. A similar voltage-step (Vstep = 1V) and computation time-venture for MPPT and FPPT calculations (Tstep = 0.2 s. i.e., the count transfer speed of the FPPT calculation is 5Hz) are considered on the whole of the contextual investigations to give a reasonable examination.

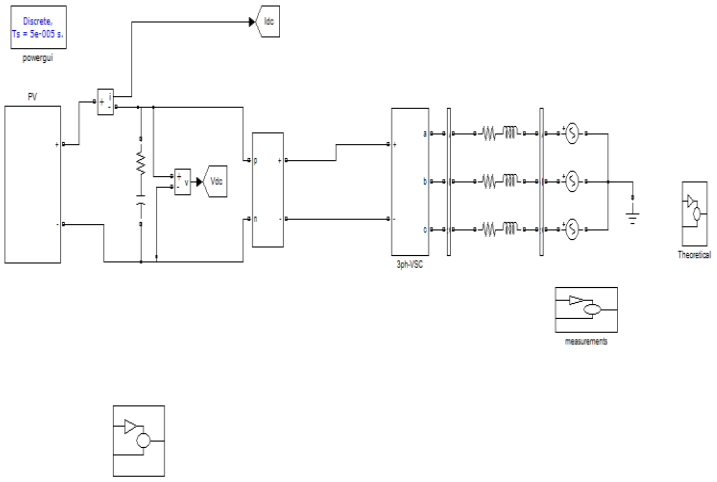

Fig 10 . simulation digram of FPPT based GCPVPP

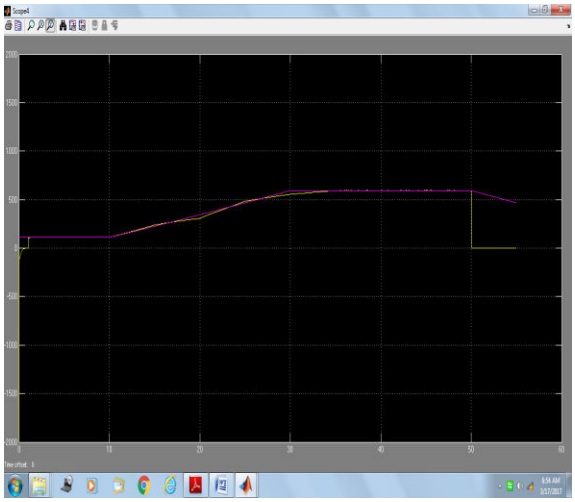

Fig 11 Simulation Result

To acquire a mathematical correlation between the exhibitions of these calculations, two boundaries are examined in the test results: first, settling season of the regulator, which is the time passed between when the accessible PV power is equivalent to or bigger than pfpp to the time that the PV power enters and stays inside a 5% mistake band of its reference worth; and second, normal following blunder in level of the

International Journal For Advanced Research In Science & Technology
A peer reviewed international journal
www.ijarst.in
ISSN: 2457-0362

absolute energy yield (T.E.), which is determined as follows [2]:

7.CONCLUSION

The exhibition of the proposed multi-mode FPPT calculation is assessed on a downsized two-stage GCPVPP. To stay away from potential slip-ups of the traditional P&O calculation because of the quick evolving illumination, this undertaking has proposed an improved FPPT regulator without PV exhibit power estimation. Our control plot utilizes the d-pivot lattice current part and the sign blunder of the PI external voltage controller. This FPPT strategy licenses one to separate the commitment of augmentation irritation and light change in force variety, thus recognizing the right heading of the MPP. The dc-connect voltage is 170V and the regulator is executed on the Boom box control stage. Two contextual investigations with the development of activity highlight the right-and left-hand sides of the MPP are performed under quick irradiance changes. To check the exhibition of the calculation proposed in this letter (alluded to as Method 1), the outcomes are contrasted and the calculation of [3], [8], and [9] (alluded to as Method 2). In Method 2, the PV voltage reference is determined straightforwardly by means of a FPPT calculation, which depends on the adjustment of the P&O calculation. A similar voltage-step (Vstep = 1V) and count time-venture for MPPT and FPPT calculations (Tstep = 0.2 s. i.e., the estimation data transfer capacity of the FPPT calculation is 5Hz) are considered altogether of the contextual analyses to give a reasonable correlation. To get a mathematical correlation between the exhibitions of these calculations, two boundaries are investigated in the exploratory outcomes: first, settling season of the regulator, which is the time slipped by between when the accessible PV power is equivalent to or bigger than pfpp to the time that the PV power enters and stays inside a 5% mistake band of its reference worth; and second, normal following blunder in level of the all out energy.

Case I: The exhibition of the proposed calculation for the development of the activity highlight the right-hand side of MPP is assessed for this situation study and results are introduced in Fig. 4. At first, the irradiance is Irr = 300 W/m2 and the greatest accessible PV power is pavai = 240 W. From t = 5 s to t = 7.8 s, the irradiance increments straightly from 300 to 1000 W/m2. Correspondingly, the accessible PV power ascends from 240 to 800W. In this way, the irradiance stays consistent at 1000 W/m2 for a term of 25 s until t = 32.8 s, in which it begins to decrease to 300 W/m2 for a transient time of 2.8 s. The greatest accessible PV power under this condition is appeared in Fig. 4(a). The force reference for the FPPT calculation (pfpp) is 500Win this contextual analysis. The PV power bends under the execution of the proposed calculation (ppvm1) and Method 2 (ppvm2) are outlined in Fig. 4(a). On the off chance that the accessible PV power is more modest than pfpp, the calculations extricate the greatest force from the PV strings. The PV power overshoot by the execution of the proposed calculation is generally little, though the overshoot under Method 2 is moderately huge. The prevalent presentation of the proposed calculation is accomplished on the grounds that the PV voltage is adaptively determined through the PI regulator.

REFERENCES

[1] Energinet.dk, "Technical regulation 3.2.2 for PV power plants with a power output

above 11 kW," Energinet.dk, Erritsø, Denmark, Tech. Rep. 14/17997-39, 2015.
[2] Y. Yang, F. Blaabjerg, and Z. Zou, "Benchmarking of grid fault modes in single-phase grid-connected photovoltaic systems," IEEE Trans. Ind. Appl., vol. 49, no. 5, pp. 2167–2176, Sep. 2013.
[3] H. D. Tafti, A. I. Maswood, G. Konstantinou, J. Pou, and F. Blaabjerg, "A general constant power generation algorithm for photovoltaic systems," IEEE Trans. Power Electron., vol. 33, no. 5, pp. 4088–4101, May 2018.
[4] H. D. Tafti, A. Sangwongwanich, Y. Yang, J. Pou, G. Konstantinou, and F. Blaabjerg, "An adaptive control scheme for flexible power point tracking in photovoltaic systems," IEEE Trans. Power Electron., 2018, to be published, doi: 10.1109/TPEL.2018.2869172.
[5] H. D. Tafti et al., "Study on the low-voltage ride-thorough capability of photovoltaic grid-connected neutral-point-clamped inverters with active/ reactive power injection," IET Renewable Power Gener., vol. 11, no. 8, pp. 1182–1190, Jul. 2017.
[6] H. D. Tafti, A. I. Maswood, G. Konstantinou, J. Pou, and P. Acuna, "Active/reactive power control of photovoltaic grid-tied inverters with peak current limitation and zero active power oscillation during unbalanced voltage sags," IET Power Electron., vol. 11, no. 6, pp. 1066–1073,
May 2018.
[7] M.Mirhosseini, J. Pou, and V. G. Agelidis, "Single- and two-stage inverterbased grid-connected photovoltaic power plants with ride-through capability under grid faults," IEEE Trans. Sustain. Energy, vol. 6, no. 3, pp. 1150– 1159, Jul. 2015.
[8] A. Sangwongwanich, Y. Yang, and F. Blaabjerg, "High-performance constant power generation in grid-connected PV systems," IEEE Trans. Power Electron., vol. 31, no. 3, pp. 1822–1825, Mar. 2016.
[9] H. D. Tafti, A. Sangwongwanich, Y. Yang, G. Konstantinou, J. Pou, and F. Blaabjerg, "A general algorithm for flexible active power control of photovoltaic systems," in Proc. IEEE Appl. Power Electron. Conf. Expo., Mar. 2018, pp. 1115–1121.